Chemistry of Materials **2019**, *31*, 8957-8968

Universiteit Utrecht

ParisTech
L'ÉCOLE NATIONALE SUPÉRIEURE
DE CHIMIE DE PARIS

PSL
RESEARCH UNIVERSITY PARIS

This paper must be cited as:
Wylezich, T., Sontakke, A. D., Castaing, V., Suta, M., Viana, B., Meijerink, A., Kunkel, N., Chemistry of Materials 2019, 31, 8957-8968; doi:10.1021/acs.chemmater.9b03048.

One Ion, Many Facets: Efficient, Structurally and Thermally Sensitive Luminescence of Eu^{2+} in Binary and Ternary Strontium Borohydride Chlorides

by Thomas Wylezich,[a] Atul D. Sontakke,[b] Victor Castaing,[c] Markus Suta,[b] Bruno Viana,[c] Andries Meijerink,[b] and Nathalie Kunkel[*] [a,d]

a. Chair for Inorganic Chemistry with Focus on Novel Materials, Department of Chemistry, Technical University of Munich, Lichtenbergstr. 4, 85747 Garching, Germany.

b. Condensed Matter and Interfaces, Debye Institute for Nanomaterials Science, Department of Chemistry, Utrecht University, Princetonplein 1, 3584 CC Utrecht, Netherlands.

c. Chimie ParisTech, PSL University, CNRS, Institut de Recherche de Chimie Paris, 11 rue Pierre et Marie Curie, 75005 Paris, France.

d. Institut für Anorganische Chemie, Georg-August-Universität Göttingen, Tammannstrasse 4, 37077 Göttingen, Germany.
[*]E-mail: nathalie.kunkel@uni-goettingen.de

This document is the unedited Author's version of a Submitted Work that was subsequently accepted for publication in *Chemistry of Materials*, copyright © American Chemical Society after peer review. To access the final edited and published work see https://doi.org/10.1021/acs.chemmater.9b03048.

Abstract

The Eu^{2+}-doped mixed alkaline metal strontium borohydride chlorides $ASr(BH_4)_{3-x}Cl_x$ (A = K, Rb, Cs) and Eu^{2+}-doped strontium borohydride chloride $Sr(BH_4)_{2-x}Cl_x$ have been prepared by mechanochemical synthesis. Intense blue photoluminescence for $Sr(BH_4)_{2-x}Cl_x$ (λ_{em}= 457 nm) and cyan photoluminescence for the perovskite-type mixed alkaline metal strontium borohydride chlorides $ASr(BH_4)_{3-x}Cl_x$ (A = K, Rb, Cs) (λ_{em} = 490 nm) is already observable after short milling times. Temperature dependent luminescence measurements reveal an appreciable blue shift with increasing temperature for all $ASr(BH_4)_{3-x}Cl_x$ (A = K, Rb, Cs) until 500 K. This extremely large shift, caused by structural relaxation, as well as the vibrationally induced emission band broadening can serve as a sensitive response signal for temperature sensing, and this unique behavior has, to the best of our knowledge, not been reported in any Eu^{2+} doped phosphor so far. Additionally, bright luminescence, high quantum efficiencies, and very low thermal quenching of these Eu^{2+}-doped borohydrides show that such host materials could serve in solid state lighting applications.

Introduction

Applications of rare earth-doped inorganic materials are manifold, ranging from solid state lighting to scintillators, lasers, biomedical applications, multiphoton processes, temperature sensing, quantum information technology and many more.[1-11] Especially the $4f^{n-1}5d$-$4f^n$ transitions of Eu^{2+} (n = 7) and Ce^{3+} (n = 1) are of great importance for phosphors used in phosphor-converted light-emitting diodes (pc-LEDs).[1, 4, 12, 13] They usually show high emission intensities and also a strong dependence of the emission energy on the host material. While Eu^{2+} and Ce^{3+} emission in a number of host materials ranging from halides to nitrides has been studied for some time,[14-16] hydride, borohydride and mixed anionic hydrides have only been considered as host lattices recently.[17]

For instance, the hydride perovskites $LiMH_3$ and $LiMD_3$ (M = Sr, Ba) doped with Eu^{2+} have been thoroughly studied using luminescence, thermoluminescence, electron paramagnetic resonance and electron nuclear double resonance spectroscopy.[18-22] In particular, well-resolved vibrational fine structures of the Eu^{2+}-based emission bands is observable in these compounds and it was shown that the high polarizability of the hydride anion leads to the hitherto largest redshifts of the energies of the lowest excited $4f^65d^1$ electronic levels among all known inorganic host compounds. Besides ionic hydrides, also Eu^{2+}-doped borohydrides and mixed-anionic hydrides have been studied lately.

A general finding is that in borohydrides the emission energies of the Eu^{2+}-based $4f^65d^1$-$4f^7$ emission so far are rather comparable with those observed typically in halides. For instance, broad blue luminescence and a quantum yield of 75% was reported for $[Eu(BH_4)_2(THF)_2]$ [23] and different shades of blue were also reported for an Eu^{2+}-related emission in the perovskite-analogue borohydrides $RbEu(BH_4)_3$, $CsEu(BH_4)_3$ or $CsCa(BH_4)_3$:Eu^{2+}.[24, 25] On the other hand, recently, particular interest has grown on mixed anionic hydrides. In those compounds, the Eu^{2+}-based emission energies strongly depend on the type and number of anions other than hydride. Examples for various classes of compounds are hydride fluorides,[26-28] hydride chlorides,[29, 30] hydride oxide chlorides,[31] and even silicate hydrides.[32] In oxide hydrides, only luminescence of trivalent terbium and europium ions has been investigated so far.[33]

In this work, we present the luminescence properties of the Eu^{2+}-doped strontium borohydride chloride $Sr(BH_4)_{2-x}Cl_x$:Eu^{2+} and the alkaline metal strontium borohydride chlorides $ASr(BH_4)_{3-x}Cl_x$:Eu^{2+} (A = K, Rb, Cs) for the first time. All discussed ternary compounds show efficient cyan emission at room temperature as well as a strongly temperature-dependent shift of the emission energies. This unusually strong response of the luminescence properties of Eu^{2+} with

https://doi.org/10.1021/acs.chemmater.9b03048

regard to temperature changes may be interesting for potential applications in the field of thermometry.

Experimental section

Synthesis. Due to moisture and air sensitivity all compounds were handled in an argon-filled glove box. The mixed metal borohydrides $A Sr(BH_4)_{3-x}Cl_x:Eu^{2+}$ (A = K, Rb, Cs) were prepared via mechanochemical reaction of $LiBH_4$ (Alfa Aesar, 95%), $SrCl_2$ (Alfa Aesar, 99.995%), the corresponding alkaline borohydrides (KBH_4, Alfa Aesar 98%; $RbBH_4$ and $CsBH_4$ prepared from Rb or Cs metal and $NaBH_4$ in ethanol according to the procedure described in Ref 34) as well as EuH_2 (2 mol% doping; synthesized via hydrogenation of europium metal in an autoclave made from hydrogen-resistant Böhler L718 alloy) in a Fritsch Pulverisette Premium Line 7 in a ZrO_2 bowl with an overpressure valve. $Sr(BH_4)_{2-x}Cl_x:Eu^{2+}$ was prepared via mechanochemical reaction of stoichiometric amounts of $SrCl_2$, $LiBH_4$ and 2 mol% EuH_2. 10 ZrO_2 balls with a diameter of 10 mm are used together with approximately 0.3 g of reactants. Caution! Overpressure may build up during milling via decomposition of the borohydrides. Reactants were milled during 19 cycles with 2 minutes of milling at 600 rpm followed by 3 minutes pauses to prevent heating of the samples. To increase crystallinity, the samples were annealed at 200 °C in fused silica ampoules for 2 days.

Powder x-ray diffraction (XRD). For powder XRD analysis, a STOE STADI P diffractometer (Cu-$K_{\alpha1}$ radiation, λ = 1.54051 Å (determined from a silicon standard)), Ge-(111)-monochromator) including a DECTRIS Mythen 1 K detector was used. Samples were enclosed in 0.3 mm glass capillaries. Data was collected in the range of 2θ= 10° - 100° within 2 hours. Structural analysis was performed with the program package Topas V5 [35] and the fundamental parameter approach.[36] Cell parameters, atomic positions of the metal atoms, hydrogen and chlorine content, thermal displacement parameters, zero shift, background, size and strain parameters were refined.

Temperature dependent XRD patterns from 140 K to 290 K with intermediate steps of 25 K were recorded on a STOE IPDS 2T single crystal diffractometer in powder acquisition mode with Mo-radiation (λ = 0.71073 Å). Samples were prepared in 0.3 mm capillaries and measured over 3 min per “temperature step” with an imaging plate distance of 200 mm resulting in a diffraction range of 2θ = 4° - 35°.

Luminescence spectroscopy. Due to moisture and air sensitivity, all samples were enclosed in silica ampoules (5 mm diameter).

Photoluminescence excitation spectra at room temperature were recorded using a Xenon plasma lamp (Energetic EQ99X) with a Jobin-Yvon HR 250 monochromator (1200 grooves/mm) for excitation and an Acton Spectra Pro 2150 Dual Grating Monochromator together with a Pixis 100 CCD camera for detection. Photoluminescence excitation and emission spectra at 4.2 K were acquired with a Xenon arc lamp (450 W), an Edinburgh FLS920 spectrofluorometer with a single 0.25 m monochromator combined with appropriate band pass and long pass filters. Emission was detected with a Hamamatsu R928 photomultiplier tube (PMT). The samples were cooled with an Oxford Instruments liquid He flow cryostat with external temperature control unit. All emission spectra were corrected for the wavelength-dependent PMT sensitivity and monochromator light output while excitation spectra were corrected for the reference signal of the Xe lamp.

Temperature-dependent photoluminescence emission measurements were carried out from 14 K to 490 K in a Sumitomo Cryogenics HC-4E closed-cycle cryostat with a Lakeshore 340 temperature controller. A xenon lamp (Energetic EQ99X) was used as excitation source and spectra were recorded using an Acton Spectra Pro 2150 Dual Grating Monochromator (300

https://doi.org/10.1021/acs.chemmater.9b03048

grooves/mm, 550 nm center wavelength) and a Princeton Instruments PI 100 CCD camera. The samples were attached to a cold finger with aid of silver paint and copper tape.
Quantum yields were measured on a Hamamatsu Quantaurus-QY Absolute PL quantum yield spectrometer equipped with a 150 W xenon light source, a Czerny-Turner type spectroscope and a spectralon coated Ulbricht sphere. Ampoules containing borohydrides were opened prior to the measurements and powders were transferred immediately to the integrating sphere for measurements.
Thermal analysis (DSC). The differential scanning calorimetry (DSC) measurements were carried out using a Netzsch DSC 200 F3 Maja calorimeter in the temperature range from 295 K to 673 K and nitrogen atmosphere with heating and cooling rates of 10 K/min. Approximately 5 mg of the samples were loaded into aluminium crucibles and sealed with a press (Netzsch).

Results and discussion

Synthesis and crystal structure. The alkaline metal strontium borohydride chlorides $A\mathrm{Sr}(\mathrm{BH_4})_{3-x}\mathrm{Cl}_x$ (*A* = K, Rb, Cs) were obtained from the mechanochemical metathesis reaction of lithium borohydride, the alkaline metal borohydride and strontium chloride according to the following equation:

$$2\ \mathrm{LiBH_4} + A\mathrm{BH_4} + \mathrm{SrCl_2} \rightarrow A\mathrm{Sr}(\mathrm{BH_4})_{3-x}\mathrm{Cl}_x + (2-x)\ \mathrm{LiCl} + x\ \mathrm{LiBH_4} \qquad (1)$$

with *A* = K, Rb, or Cs. For Eu^{2+}-doped samples, EuH_2 was added (2 mol%). Mechanochemical metathesis reactions of this kind are a well-known tool for the synthesis of mixed-anion and mixed-cation borohydrides.[25, 37-40]
$A\mathrm{Sr}(\mathrm{BH_4})_{3-x}\mathrm{Cl}_x$ (*A* = K, Rb, Cs) crystallize in perovskite-related orthorhombic structures as reported before for the pure borohydrides $A\mathrm{Sr}(\mathrm{BH_4})_3$ (*A* = K, Rb, Cs) by Møller *et al.*[41] In $A\mathrm{Sr}(\mathrm{BH_4})_3$ (*A* = K, Rb, Cs) the Sr^{2+} ions are surrounded by 6 $[\mathrm{BH_4}]^-$ - tetrahedra forming a distorted octahedron. These octahedra are connected via corners to build up a three-dimensional network. The structure of $\mathrm{KSr}(\mathrm{BH_4})_3$ is shown in Fig. 1 (for *A* = Rb, Cs see Fig. S1 in the Supporting Information). All three compounds share the same structural motif. Due to the similar ionic radii of Sr^{2+} and Eu^{2+},[42] it can be expected that Eu^{2+} occupies the strontium site and is therefore coordinated by a distorted octahedron of $[\mathrm{BH_4}]^-$ units.

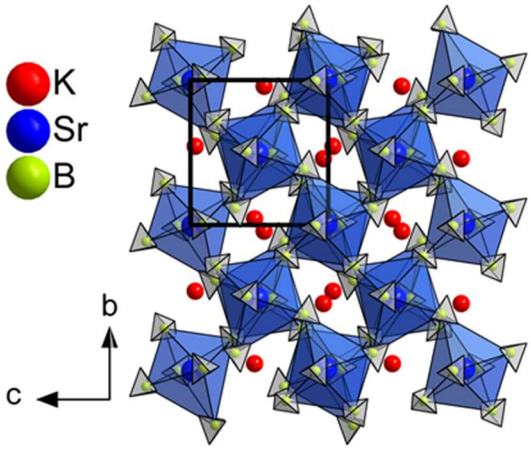

Figure 1: Representative crystal structure of $\mathrm{KSr}(\mathrm{BH_4})_3$ according to Ref. 41. Sr (blue) is coordinated by six $[\mathrm{BH_4}]^-$ tetrahedra (grey) building up a three-dimensional network. Hydrogen atoms of the $[\mathrm{BH_4}]^-$ units are omitted for clarity.

Table 1 summarizes selected structural information for $A\mathrm{Sr}(\mathrm{BH_4})_{3-x}\mathrm{Cl}_x$ (*A* = K, Rb, Cs) and $\mathrm{Sr}(\mathrm{BH_4})_{2-x}\mathrm{Cl}_x$ obtained from Rietveld refinement. A detailed list of the atomic positions is given in the Supporting Information, Table S1.
For the chloride content *x*, 0.20, 0.14, and 0.26 were obtained for *A* = K, Rb, and Cs, respectively. The partial chloride substitution in mixed metal borohydrides prepared by

mechanochemical milling is in good agreement with previously reported works.[25, 39] Exemplarily, the Rietveld refinement of the structure of $KSr(BH_4)_{2.80}Cl_{0.20}$ is shown in Fig. 2. Additional Rietveld refinements of the structures of $Sr(BH_4)_{1.74}Cl_{0.26}$, $RbSr(BH_4)_{2.86}Cl_{0.14}$ and $CsSr(BH_4)_{2.74}Cl_{0.26}$ are compiled in Figs. S2 – S4 of the Supporting Information.

Table 1: Crystallographic information for the mixed metal borohydrides $ASr(BH_4)_{3-x}Cl_x$ (*A* = K, Rb, Cs) and $Sr(BH_4)_{2-x}Cl_x$.

Compound	**$KSr(BH_4)_{3-x}Cl_x$**	**$RbSr(BH_4)_{3-x}Cl_x$**	**$CsSr(BH_4)_{3-x}Cl_x$**	**$Sr(BH_4)_{2-x}Cl_x$**
Space group	*P* 2_1 *c n* (33)	*P b n* 2_1 (33)	*P* 2 2_1 2_1 (18)	*P b c n* (60)
Cell parameters [Å]				
a	11.3749	8.2717	6.0840	6.9160
b	8.3074	8.0830	8.0941	8.3096
c	7.5106	11.5538	8.0867	7.5129
***d*(Sr – B) [Å]**	2.71 – 3.54	2.38 – 3.65	2.84 – 3.24	2.96 – 3.13
d_{avg}(Sr – B) [Å]	3.06 ± 0.12	3.00 ± 0.17	3.01 ± 0.06	3.02 ± 0.08
CN (Sr)	6	6	6	6
***x* (via Rietveld)**	0.20	0.14	0.26	0.26

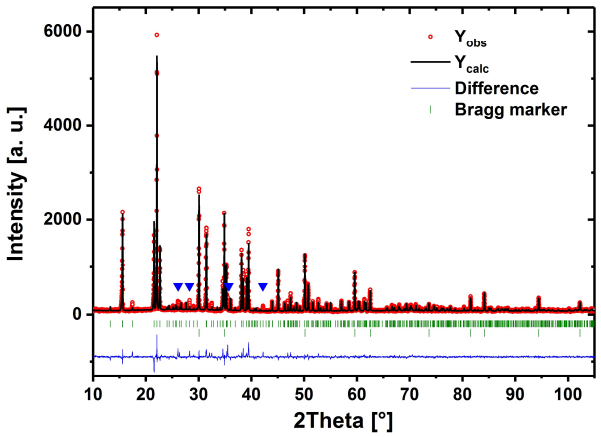

Figure 2: Rietveld refinement of $KSr(BH_4)_{3-x}Cl_x$. Structural refinement yields a substitution of $[BH_4]^-$ - units with Cl^- of *x* = 0.20. After ball milling approx. 32 wt% of LiCl is obtained as a secondary phase, blue triangles mark a non-identifiable phase. Bragg markers from top to bottom: $KSr(BH_4)_{2.80}Cl_{0.20}$, LiCl.

$Sr(BH_4)_{1.74}Cl_{0.26}$:Eu^{2+} was obtained from the mechanochemical reaction of $SrCl_2$ with two equivalents of $LiBH_4$ and 2 mol% EuH_2 for Eu^{2+}-doping as reported by Ravnsbæk *et al.*[39] $Sr(BH_4)_2$ crystallizes orthorhombically in space group *Pbcn* and Sr is coordinated by six $[BH_4]^-$ - units, which form a slightly distorted octahedron.

For $KSr(BH_4)_{2.80}Cl_{0.20}$, a DSC measurement showed no phase transition in the range of -160°C to 250°C (see Fig. S14 in the Supporting Information). At 252°C, an endothermic signal indicates the decomposition at much lower temperatures compared to the pure borohydride analogue $KSr(BH_4)_3$ reported by Møller *et al.*,[41] which decomposes at approximately 400°C. Møller *et al.* suggested that at 258°C, a structural transformation to a HT-polymorph of $KSr(BH_4)_3$ occurs. The authors came to that conclusion based on additional reflections observed in high temperature synchrotron diffraction patterns. Yet, in their DSC measurements they did not observe any heat flow changes in the corresponding temperature range, but only a strong endothermic signal at 400°C. The borohydride chloride $KSr(BH_4)_{2.80}Cl_{0.20}$ presented in this work, in turn, does not show any strong signal at 400°C, but at significantly lower temperature (252°C), which suggests decomposition as also confirmed by *ex-situ* XRD. For

samples that were heated to 250°C and 300°C, respectively, XRD analysis showed two phases of $KSr(BH_4)_{3-x}Cl_x$ with different *x* values at 250°C (see Fig. S5 in the supporting info). At 300°C, the sample clearly darkened and only one $KSr(BH_4)_{3-x}Cl_x$ phase is present. After treatment at 400°C, the powder appeared black, which suggests a decomposition of the remaining phase at higher temperatures.

Temperature-dependent crystal structure data from X-ray powder diffraction patterns collected on a single crystal diffractometer from 140 K to room temperature showed a temperature dependence of the lattice parameters for the mixed metal borohydride chlorides $ASr(BH_4)_{3-x}Cl_x$ (*A* = K, Rb, Cs) (see Fig. S6 to S13 in the supporting information). In the range between room temperature and 600 K, DSC and *ex-situ* X-ray diffraction was used. For all ions *A*, an increase of temperature results in a linear increase of the cell parameters. Accordingly, positive volumetric thermal expansion coefficients can be deduced, namely 14.5 x 10^{-5} K^{-1} (*A* = K), 9.2 x 10^{-5} K^{-1} (*A* = Rb) and 6.9 x 10^{-5} K^{-1} (*A* = Cs) according to equation (2),

$$\alpha_V = \frac{1}{V}\left(\frac{\partial V}{\partial T}\right)_p \qquad (2)$$

where the subscript indicates constant (ambient) pressure conditions. The magnitude of the thermal expansion coefficient is particularly related to the anisotropy in different bonds within a given crystal or, alternatively, the increasing degree of anharmonicity of the respective collective vibrations. According to the crystal structure data of the pure ternary borohydrides, the decreasing magnitude from *A* = K to *A* = Cs also becomes readily evident upon already regarding the coordination sphere of the Sr^{2+} ions as a representative example: the coordination spheres of the $[Sr(BH_4)_6]^{4-}$ octahedra become less distorted upon variation of *A* = K to *A* = Cs. This critical point will be reviewed in terms of its effects on the photoluminescence properties of Eu^{2+} below in detail.

Luminescence spectroscopy. After short milling times of only 90 min at 600 rpm the Eu^{2+}-doped samples already exhibit intense cyan luminescence in mixed cationic borohydride-chlorides and blue in Sr-borohydride-chloride under UV excitation (Fig. 3)

Figure 3: Photographs of $ASr(BH_4)_{3-x}Cl_x$ (*A* = K, Rb, Cs; *x* = 0.20, 0.14, 0.26) and $Sr(BH_4)_{2-x}Cl_x$ (*x* = 0.26) from left to right. *Top*: Samples under daylight, *bottom*: Samples under 365 nm excitation in an argon filled glovebox.

https://doi.org/10.1021/acs.chemmater.9b03048

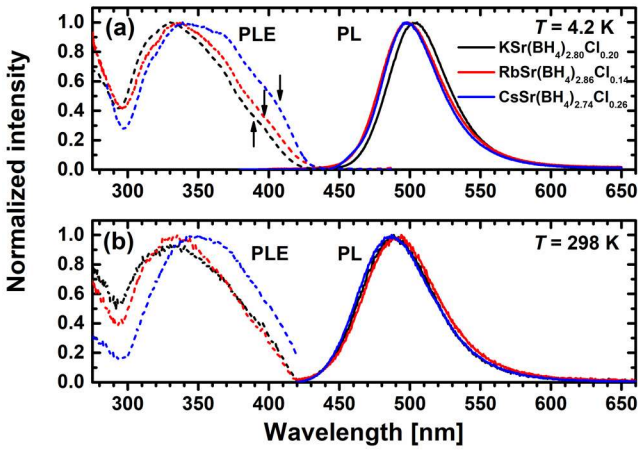

Figure 4: (a) Photoluminescence excitation (dashed) and emission spectra (solid) of Eu^{2+} in $ASr(BH_4)_{3-x}Cl_x$ (A = K, Rb, Cs; x = 0.20, 0.14, 0.26) at 4.2 K **(b)** same measurements at room temperature. For λ_{ex} and λ_{em} of the respective spectra, see Table 2. The arrows mark the estimated positions of the emissive $4f^6(^7F_0)5d^1$ states.

Table 2: Characteristic optical parameters deduced from the photoluminescence spectra of $ASr(BH_4)_{3-x}Cl_x$ (A = K, Rb, Cs; x = 0.20, 0.14, 0.26). Values refer to 4.2 K if not noted otherwise.

Compound	Excitation maximum		Emission maximum		Zero phonon line (ZPL)		FWHM	Stokes shift	Decay time[b]
	[nm]	[cm^{-1}][a]	[nm]	[cm^{-1}][a]	[nm]	[cm^{-1}][a]	[cm^{-1}][a]	[cm^{-1}][a]	[ns]
$KSr(BH_4)_{2.80}Cl_{0.20}$	330	29690	504	19830	436	22630	1970	5600	608
$RbSr(BH_4)_{2.86}Cl_{0.14}$	335	29130	499	19990	438	22565	2085	5140	598
$CsSr(BH_4)_{2.74}Cl_{0.26}$	339	27270	497	20000	444	22400	1940	4800	558

[a] Obtained by proper conversion of the photon counts per constant wavelength interval into wavenumber domain by inclusion of the factor $\left|\frac{d\tilde{\nu}}{d\lambda}\right| = \frac{1}{\lambda^2}$.

[b] Values refer to room temperature.

Figure 4 depicts the photoluminescence excitation and emission spectra of $ASr(BH_4)_{3-x}Cl_x$ (A = K, Rb, Cs; x = 0.20, 0.14, 0.26) at 4.2 K and room temperature after having annealed the samples at 200°C for 2 days. All three Eu^{2+}-activated ternary borohydride compounds show a broad emission located in the cyan range at around 490 – 500 nm. The broad banded appearance of the emission is typical for the parity-allowed $4f^65d^1$ – $4f^7$ transition of Eu^{2+}. Similar emission spectra have been previously recorded by Schouwink *et al.*[24, 25] in the mixed borohydrides $CsCa(BH_4)_3$:Eu^{2+} and $CsEu(BH_4)_3$ that were also prepared by mechanochemical synthesis. Another example is the molecular compound $[Eu(BH_4)_2(THF)_2]$ reported by Marks *et al.*[23] In contrast, there is only the corresponding chloride analogue $CsSrCl_3$:Eu^{2+} reported to show the respective $4f^65d^1 \rightarrow 4f^7$ emission transition at around 431 nm.[43,44] Since Rietveld analyses result in low chloride substitution for the here reported mixed anionic alkaline metal strontium borohydride chlorides the photoluminescence properties origin mainly from the borohydride ligands and, as will also argued below, the Cl^- ligands only have a negligible effect thereon.

The maxima in the photoluminescence excitation spectra of these compounds are systematically redshifted from K (330 nm) over Rb (335 nm) to Cs (339 nm) and exhibit a broadened fine structure both at 4.2 K and room temperature (see Figure 4.(a), (b), dashed lines). The fine structure is related to the underlying spin-orbit splitting of the $4f^6$ core into the different ^7F_J (J = 0…6) levels in the excited $4f^65d^1$ configuration. In contrast to strongly ionic compounds exhibiting a well-resolved fine structure due to these levels,[45,46] the limited resolution even at 4.2 K indicates a larger degree of covalency of the Eu-BH_4 bonds and a correspondingly stronger electronic interaction between the $4f^6$ core and 5d electron. In addition, relaxation in the excited state giving rise to a relatively large Stokes shift (*vide infra*)

https://doi.org/10.1021/acs.chemmater.9b03048

also results in significant broadening of all $4f^7 \rightarrow 4f^6(^7F_J)5d^1$ excitation bands and also contributes to the absence of clearly resolved ^7F_J fine structure.

The gradual redshift of the excitation maximum from the K- to Cs-based compound may be asserted by a repulsive effect of the second coordination sphere on the Eu^{2+} ions and thus, counteracting destabilization of the excited $4f^65d^1$ configuration. Since K^+ ions are smaller than Rb^+ and Cs^+ ions, the former may approach the Eu^{2+} ions more closely.[42] The alike positive charge then leads to a repulsive contribution, which in turn destabilizes the $4f^65d^1$ configuration and should in total induce a higher energy of that configuration in the K-based compound compared to the energy in the Cs-based compound. This interpretation is additionally suggested by various longer and more anisotropic Sr-B bond lengths in the ground state structure of the K representative compared to the Cs representative (see also Table 1 and Figure 5).

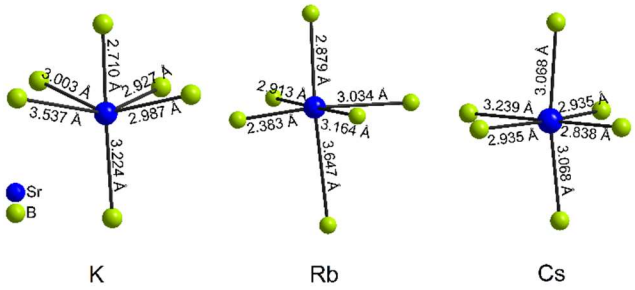

Figure 5: Bond lengths of the three ternary strontium borohydride chlorides in the respective $[Sr(BH_4)_6]$ octahedra. The structural anisotropy of the octahedra decreases from K over Rb to Cs. Hydrogen atoms are omitted for clarity.

In line with the consequences of such a repulsive impact, excitation from a very localized and shielded $4f^7$ configuration of Eu^{2+} to a more open or covalent $4f^65d^1$ configuration should induce a higher degree of excited state relaxation in the K-based compound to allow the ligand field to minimize its energy with respect to this higher degree of Coulomb repulsion. Thus, it is expected that the bond length in the excited $4f^65d^1$ configuration changes more strongly for *A* = K than for *A* = Cs. This is in line with the observed trend of Stokes shifts (see Table 2). Due to the higher number of different excited states underlying the broad excitation bands of Eu^{2+}, an accurate determination of the Stokes shift for this divalent lanthanide ion is far from trivial and typically only approximately possible. Based on the positions of the zero-phonon lines (ZPLs) determined by the crossing point between emission and excitation spectra at 4.2 K (see Figure 4.(a)), the Stokes shifts are estimated to ΔS = 5600 cm^{-1}, 5140 cm^{-1} and 4800 cm^{-1} for *A* = K, Rb and Cs, respectively. Besides the expected decreasing trend from *A* = K to Cs and the connected successive symmetrisation of the coordination sphere of Eu^{2+}, these values reasonably assess the position of the emissive $4f^6(^7F_0)5d^1$ state assuming a valid interpretation of decoupled interaction scheme between 4f and 5d electrons (see arrows in Figure 4.(a)) as the lowest energetic shoulders of the broad excitation bands.

Another measure for the non-radiative relaxation in the excited $4f^65d^1$ configuration is the emission bandwidth of the corresponding $4f^65d^1 \rightarrow 4f^7$ transition. In contrast to the Stokes shift, it can be accurately determined over the whole temperature range between 4.2 K to around 500 K and is often in the same order of magnitude as the Stokes shift. For the considered Eu^{2+}-activated borohydride chlorides, the corresponding full widths at half maximum (FWHMs) read 1970 cm^{-1} for *A* = K, 2085 cm^{-1} for *A* = Rb and 1940 cm^{-1} for *A* = Cs (see also Table 2). Interestingly, the Eu^{2+}-related emission band FWHM in the Rb representative is larger than in the other two compounds, which is a consequence of inhomogeneous broadening induced by the largest anisotropy of the Eu-B bond lengths in the first coordination sphere among all presented borohydride chlorides (see Table 1 and Figure 5). Thus, the emission band FWHMs

reflect the local structural anisotropies around the Eu^{2+} ions more accurately than the Stokes shifts do.

For a discussion of the structure-luminescence relationship of Eu^{2+}, the emission spectra of Eu^{2+} at 4.2 K have to be regarded (see Figure 4.(a), solid lines). The emission maxima shift from 504 nm for *A* = K over 499 nm for *A* = Rb to 497 nm for *A* = Cs to systematically higher energies. This behaviour is also in agreement with the previous discussion on the variation of the excitation energies and Stokes shifts. At room temperature, the emission bands of all three chloride borohydrides display a thermally induced blueshift and thereby strongly overlap (see Figure 4.(b)).

Only the emission spectrum of Eu^{2+} in $CsSr(BH_4)_{2.74}Cl_{0.26}$ at 4.2 K displays a partially resolved vibrational fine structure at the higher energy side. The lacking resolution may be partially attributed to the presence of the Cl^- ions that induce inhomogeneous broadening effects, but also the covalent Eu-BH_4 bonds. Apart from that impact, however, the regularity in trends from both the excitation and emission spectra indicate that the Cl^- ligands do not have a significant effect on the appearance of the luminescence spectra of the presented compounds and most of the Eu^{2+} ions may be coordinated by solely $[BH_4]^-$ anions. Nonetheless, the decreasing Stokes shift from *A* = K to Cs relates to a correspondingly decreasing Huang-Rhys-Pekar parameter S_{eff} that serves as a measure for the strength of the electron-vibrational coupling and denotes the average number of vibrations emitted during the relaxation process.[47] It can be estimated from the emission spectra by comparison of the integrated intensity I_0 of the zero-phonon transition (being estimated by the crossing point between emission and excitation spectra) relative to that of the vibrational sidebands, I_p,

$$I_0 = I_p \mathrm{e}^{-S_{\text{eff}}} \tag{3}$$

It should be noted that due to the different nature of chemical bond in the $4f^7$ ($^8S_{7/2}$) and $4f^65d^1$ electronic states, respectively, also the Huang-Rhys-Pekar factors for the excitation transition and emission transition then differ, respectively. S_{eff} is then the geometric mean of these two values and a reliable effective measure, especially if it is small. Based on eq. (3), the values for S_{eff} for the different chloride borohydrides read S_{eff} = 6.3 (*A* = K), S_{eff} = 5.6 (*A* = Rb) and S_{eff} = 5.0 (*A* = Cs). It is noteworthy that the Huang-Rhys-Pekar factors already differ significantly despite the fact that the alkali ions only reside in the second coordination sphere of Eu^{2+} and thus, illustrate the yet sensitively detectable local response of the Eu^{2+}-based luminescence thereon. Additionally, a lower effective Huang-Rhys-Pekar parameter should give better resolved vibrational fine structure, which is in agreement with the observations on $CsSr(BH_4)_{2.74}Cl_{0.26}$ (*cf.* Figure 4.(a)).

From the Huang-Rhys-Pekar factors S_{eff} and the determined Stokes shifts ΔS (see Table 2), an average value for the vibrational mode that is coupled to an electronic transition is estimated by the high FWHM limit[48]

$$\Delta S = 2S_{\text{eff}}\hbar\omega_{\text{eff}} \tag{4}$$

and gives an average value of $\hbar\omega_{\text{eff}} = (460 \pm 10)$ cm^{-1} among the three Eu^{2+}-activated ternary chloride borohydrides. This value agrees very well with the observed highest energetic librational mode in the pure borohydride perovskites $ACa(BH_4)_3$[24,49] and also fits to the expectation that the electronic states of Eu^{2+} should couple to a vibrational mode that also influences the Eu-B bonds instead of internal vibrational modes of the $[BH_4]^-$ units themselves. In particular, the relevance of this librational mode for the anharmonic structural phase transitions in the pure borohydrides was emphasized.[49] Furthermore, the photoluminescence decay curves at room temperature have been recorded for $ASr(BH_4)_{3-x}Cl_x:Eu^{2+}$ (Fig. S16 – S19 Supporting Information and Table 2). In all compounds, the Eu^{2+}-based emission intensity

shows a single exponential decay and lifetimes of about 608 ns for $KSr(BH_4)_{2.80}Cl_{0.20}$, 598 ns for $RbSr(BH_4)_{2.86}Cl_{0.14}$ and 558 ns for $CsSr(BH_4)_{2.74}Cl_{0.26}$ were obtained. This is in reasonable agreement with decay times reported for the Eu^{2+} emission in metal hydrides[17], fluorides[50] or other complex oxides[51] at room temperature. Comparingly, they are shorter than the values reported for the pure halides $CsMBr_3$ and $CsMI_3$ (M = Mg, Ca, Sr) at room temperature, which are in the range of around 800 – 900 ns at room temperature instead.[45,46] This variation is attributed to an impact of non-radiative decay, which correlates with the vibrational energies of the local modes or phonons that the electronic states of the Eu^{2+} ions couple to. The vibrational coupling energy in the presented borohydride chlorides at around 460 cm^{-1} is right in between the maximum phonon energies found in fluorides or several complex oxides between 350 cm^{-1} to 700 cm^{-1},[52] thus explaining the similarity in the respective decay times of the $4f^65d^1$ configuration at room temperature. In contrast, the phonon energies of bromides and iodides are in the range of 160 cm^{-1} to 120 cm^{-1},[53] and as a result, the corresponding $4f^65d^1$-related decay times become slightly longer. An additional influence stems from photonic effects on the radiative decay time such as the refractive index inducing a local field correction in a dielectric, but also the emission wavelength ($\lambda_{\mathrm{em}}^{-3}$ dependence of the Einstein coefficient of spontaneous emission).[54] These effects become, however, only clearly distinguishable at very low temperatures when non-radiative decay is negligible.

Temperature dependent luminescence emission spectra of Eu^{2+} have been recorded for all ternary chloride borohydrides and are shown in Fig. 6. While all compounds are characterized by a vibrationally induced broadening of the emission bands (see also Fig. S23 for the temperature evolution of the full widths at half maximum), the integrated emission intensity remains very stable even up to 500 K (decrease by less than 10%, see Figures S20-S22) and indicate that despite the potentially high energetic stretching vibrations of the $[BH_4]^-$ ligands at around 2400 cm^{-1},[49] quenching of the Eu^{2+} luminescence in the chloride borohydrides is inefficient. Decomposition of the borohydrides hinder further recording of luminescence spectra above 500 K. However, the present data clearly suggest that the quenching temperature $T_{50\%}$ should be well above 500 K for *A* = K, Rb and Cs (see Figs. S20 – S22 of the Supporting Information).

Since all reported Eu^{2+}-doped compounds show very intense photoluminescence even up to 500 K, internal quantum yield measurements at room temperature were carried out to determine the efficiency of these phosphors. Table 3 compares the quantum yield for Eu^{2+} emission on $ASr(BH_4)_{2.80}Cl_{0.20}$ (*A* = K, Rb, Cs) with previously reported quantum yields in similar compounds.

Table 3: Absolute quantum yield (QY) of different Eu-containing borohydride compounds at 293 K.

Compound	**λ_{exc} [nm]**	**λ_{em} [nm]**	**Quantum yield [%]**
$KSr(BH_4)_{2.80}Cl_{0.20}:Eu^{2+}$	330	489	93
$RbSr(BH_4)_{2.86}Cl_{0.14}:Eu^{2+}$	330	492	53
$CsSr(BH_4)_{2.74}Cl_{0.26}:Eu^{2+}$	350	486	76
$[Eu(BH_4)_2(THF)_2]$ [23]	360	490	75
$[Eu(BH_4)(THF)_5][BPh_4]$ [23]	360	458	5

Among the mixed metal borohydride chlorides $ASr(BH_4)_{3-x}Cl_x$ (*A* = K, Rb, Cs), the highest efficiency is found for *A* = K with 93% internal quantum yield followed by Cs (76%) and Rb (53%). For comparison, Marks *et al*. reported an absolute quantum yield of 75% for $[Eu(BH_4)_2(THF)_2]$ and were able to increase the quantum yield to 93% by deuteration of the compound.[23]

https://doi.org/10.1021/acs.chemmater.9b03048

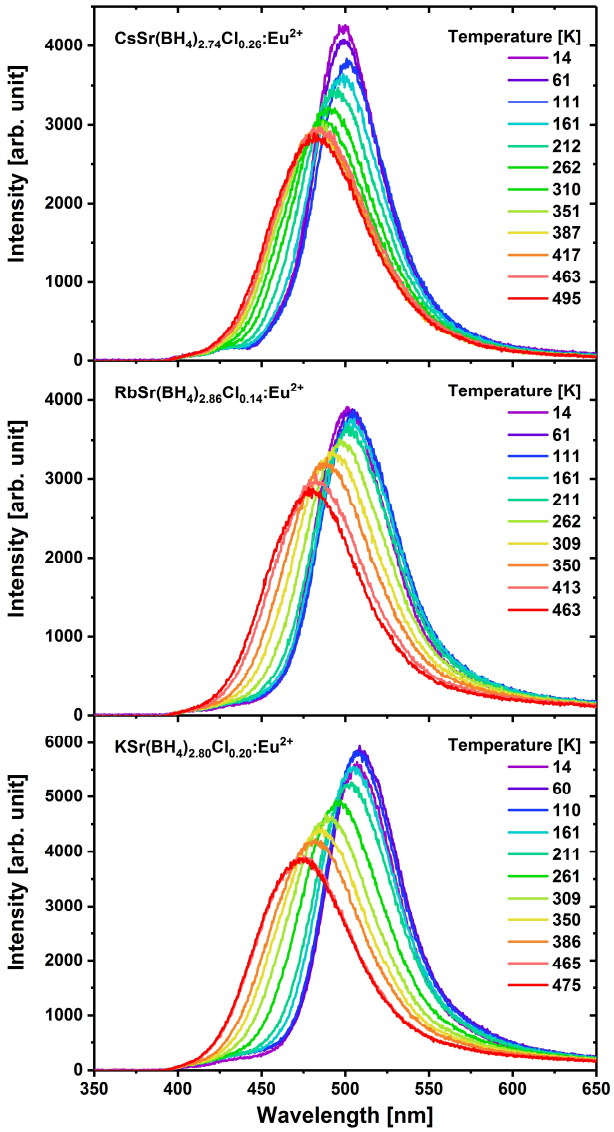

Figure 6: Temperature dependent photoluminescence spectra of the $4f^65d^1 \rightarrow 4f^7$ transition of Eu^{2+} in $CsSr(BH_4)_{2.74}Cl_{0.26}$ (top, λ_{ex} = 330 nm), $RbSr(BH_4)_{2.86}Cl_{0.14}$ (middle, λ_{ex} = 330 nm) and $KSr(BH_4)_{2.80}Cl_{0.20}$ (bottom, λ_{ex} = 350 nm) excited with a xenon lamp.

In addition to the previously characterized features of the temperature-dependent luminescence of Eu^{2+}, an extraordinary blueshift of the $4f^65d^1 \rightarrow 4f^7$-related emission maxima with increasing temperatures is observed in all three ternary mixed borohydrides $ASr(BH_4)_{3-x}Cl_x$ (see Figure 6). As depicted in Figure 7, the Eu^{2+}-based luminescence in all three compounds first display a slight redshift within the range of 15 K to 150 K, while a blueshift emerges at higher temperatures. The net blueshift of the temperature-dependent emission maxima systematically decrease from ΔE_{em} = 1500 cm^{-1} for *A* = K over ΔE_{em} = 990 cm^{-1} for *A* = Rb to ΔE_{em} = 700 cm^{-1} for *A* = Cs between 14 K and 495 K. This feature is perfectly correlated to the trend of thermal expansion coefficients as derived from the temperature-dependent XRD measurements and indicates that the Eu^{2+}-based luminescence sensitively reacts on the successively anisotropically increasing bond lengths from 140 K on (see Fig. S9, S11 and S13).

The temperature-dependent peak maxima for *A* = K, Rb and Cs are shown as a function of temperature in Fig. 7.

https://doi.org/10.1021/acs.chemmater.9b03048

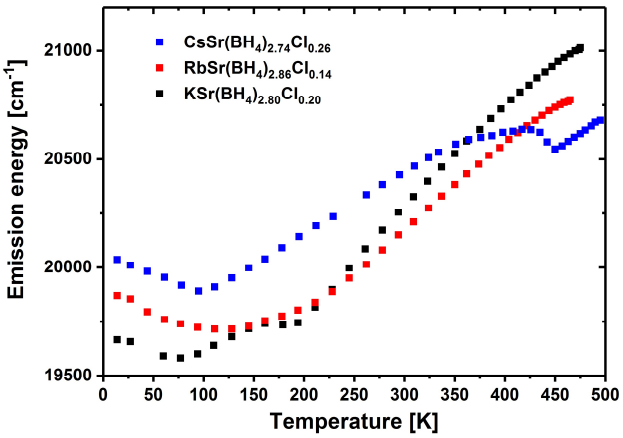

Figure 7: Temperature dependent peak maximum of the Eu^{2+} photoluminescence emission in $ASr(BH_4)_{3-x}Cl_x:Eu^{2+}$ (*A* = K, Rb, Cs; *x* = 0.20, 0.14, 0.26).

Predictions of the direction and magnitude of temperature-dependent shifts of the emission maxima in, e.g. Eu^{2+}- and Ce^{3+} activated phosphors are not always straightforward. Yan[55] proposed that one reason for the observation of a redshift can be the broadening of the emission band with increasing temperature, which may lead to an increased self-absorption due to a larger overlap of the photoluminescence excitation and emission spectra.

A blueshift, on the other hand, can have several origins. One important cause is lattice expansion, which increases the activator-ligand distance and thus, results in a smaller crystal field splitting and decreasing covalency of the lanthanide-ligand bond. Furthermore, thermally induced population of higher vibrational states may lead to a higher emission energy with increasing temperature due to the presence of hot vibrational side bands. For approximately harmonic vibronic states, however, it was shown that thermal population of higher vibrational states does not affect the energetic position of the emission maximum.[48]

In addition, also the thermal excitation into the energetically closely lying spin-orbit ^7F_J levels (J = 1, 2) of the $4f^6$ core of the excited configuration may induce a systematic blue shift and has been interpreted to occur in other Eu^{2+}-activated halides before.[45] However, given the energy difference of only 400 cm^{-1} between the $^7F_0$ and $^7F_1$ level in the $4f^6$ core,[56] this mechanism alone cannot be responsible for the significantly strong thermochromic blueshift of the Eu^{2+}-based emission observed in these mixed anionic borohydrides (see Figure 6) in the range between 1000 -1500 cm^{-1} in all three compounds. Upon comparison to conventionally observed thermochromic blueshifts of the $4f^65d^1 \rightarrow 4f^7$ configuration of Eu^{2+} in other host compounds[45, 46] in the order of only ~ 100 cm^{-1}, the presented borohydride chlorides are unique in their thermal Eu^{2+}-related photoluminescence response. For instance, such compounds could, in principle, be used as internal temperature sensors in *in situ* neutron diffraction studies where transparent reaction chambers are used.[57] Certainly, this would probably require additional pressure calibration due to the dependence of the emission on the interatomic distances and the related vibrational modes. Further options could be the encapsulation into a polymer matrix and using the particles in reaction monitoring under different atmospheres as is currently investigated for various processes for other phosphors with temperature-dependent peak positions.[58] Due to decomposition of the $KSr(BH_4)_{2.80}Cl_{0.20}:Eu^{2+}$ at higher temperatures, no luminescence emission could be studied above 500 K. The steady and sensitive blueshift as a response to external temperature changes in the region between 200 and 475 K combined with the fact that this mixed anionic borohydride does not decompose in this temperature region under atmospheric inert gas pressure or under hydrogen atmosphere make especially this compound a promising local and sensitive temperature sensor, for example during hydrogenation reactions, as will also quantitatively assessed below.

https://doi.org/10.1021/acs.chemmater.9b03048

As the $4f^65d^1$ configuration reacts sensitively to local structural changes in the coordination environment of the Eu^{2+} ions, we propose the following mechanistic explanation for the large temperature induced blueshift. At low temperatures, the bond lengths between Eu^{2+} (being as large as Sr^{2+}) and the surrounding $[BH_4]^-$ units are highly anisotropic, which give rise to a deviation from perfect octahedral symmetry of the coordination sphere of the Eu^{2+} ions. Correspondingly, the lowest energetic emissive $4f^65d^1(t_{2g})$ crystal field states of Eu^{2+} will lose their degeneracy and split up into at most three states. Since the smaller K^+ ions in the second coordination sphere may approach closer to the Eu^{2+} ions than the bulkier Rb^+ and Cs^+ ions, the Eu-B bonds in the first coordination sphere increase from the Cs to the K compound in average (see also Table 1 and Figure 5). In turn, the low symmetry splitting of the 5d orbitals of Eu^{2+} should decrease from $CsSr(BH_4)_{2.74}Cl_{0.26}$ over $RbSr(BH_4)_{2.86}Cl_{0.14}$ to $KSr(BH_4)_{2.80}Cl_{0.20}$ due to the overall increasing bond lengths in that order. Correspondingly, any excitation from the shielded $4f^7$ to the chemically more covalent $4f^65d^1$ configuration will affect the bond length most in the *A* = K-related representative, which is additionally accompanied by large Stokes shifts. This explains the energetic order of the $4f^65d^1 \rightarrow 4f^7$-based emission bands at low temperatures (see Figure 4.(a)).

If the temperature is raised, the collective vibrational motion of the host crystal (including the local coordination sphere of the Eu^{2+} ions) systematically makes the Eu-B bonds more isotropic in thermal average. Correspondingly, at some temperature, the octahedral symmetry is approximately retained and the $4f^65d^1(t_{2g})$ levels recover their degeneracy. In agreement with that picture, the emission should be systematically blueshifted and can cover larger energy difference dependent on the symmetry-induced splitting of the t_{2g} states, in agreement to observations. Alternatively, the thermally induced lattice expansion should generally increase the Eu-B bonds in average and thus, lead to a generally observable blueshift of the Eu^{2+}-related emission with increasing temperature in all three compounds. A strong indication for the relevance of vibrations for the photoluminescence properties of these compounds is given by the different magnitudes of blue shifts among the three ternary borohydride chlorides. Their values are in perfect line with the decreasing size of the thermal expansion coefficients α_V from *A* = K to *A* = Cs (see above and Figures S9, S11, S13). As the thermal expansion coefficient is an indirect measure for the response of a crystal to thermally excited (in particular, anharmonic) vibrations, it is also expected that the *A* = K representative should show the largest blueshift of the Eu^{2+}-related emission. In turn, that also implies that at a certain temperature, the three compounds should emit at around the same wavelength, which is in fact the case at around room temperature (see Figure 4.(b) or 7). At higher temperatures, it is then expected that the emission energies reverse their order and that the *A* = K should show the most blueshifted emission, also in agreement with observations.

The observed redshifts of the Eu^{2+}-based $4f^65d^1 \rightarrow 4f^7$ emission in all compounds $ASr(BH_4)_{3-x}Cl_x$ (see Figure 7) at temperatures below 150 K may be easily explained in the framework of this model if α_V is negative at those temperatures. Future studies are already ongoing to verify both this aspect and also the applicability of this model in other related compounds. Another impact can be the balance between thermally induced vibrational broadening of the emission and corresponding symmetrisation of the coordination sphere around Eu^{2+} at higher temperatures. In fact, the full widths at half maximum (FWHMs) of particularly the Rb- and Cs-based compound increase almost linearly with temperature even below 150 K, while in the K-based compound, the Eu^{2+}-based emission FWHM remains constant at those temperatures (see Fig. S23 in the Supporting Information). A hint on the validity of this balancing interpretation is the vanishing of the blueshift of the $4f^65d^1 \rightarrow 4f^7$ emission of Eu^{2+} in $KSr(BH_4)_{2.80}Cl_{0.20}$ in exactly the temperature range of constant FWHMs.

https://doi.org/10.1021/acs.chemmater.9b03048

The emission energies and europium – ligand distances found in the present work are subsequently compared to similar compounds with octahedrally coordinated europium/strontium sites and different anions reported earlier and can be seen in Table 4.

Table 4: Various europium doped strontium compounds with the coordination number (CN = 6), their emission wavelength and atomic distances *d*(Sr – X). The given atomic distances in compounds with simple anions correspond to the europium – anion distance, whereas in compounds with complex anions, the distances are given as distances between europium and the central atom of the complex anion.

Compound	*d*(Sr – X) [Å]	d_{avg}(Sr – X) [Å]	Emission [nm]	Reference
$SrSO_4$	3.40 – 3.95	3.57	378	[59]
$SrLiB_9O_{15}$	3.33 – 3.90	3.68	385 [b]	[60]
$Sr_3(PO_4)_2$	3.44	3.44	413 [c]	[61]
$Sr_3P_4O_{13}$	3.25 – 3.82	3.48	415 [d]	[62]
$CsSrBr_3$	3.05 – 3.08	3.06	428-430	[45, 63]
$CsSrI_3$	3.36	3.36	446-454	[46, 64]
$NaSrPO_4$	3.20 – 4.15	3.67	451	[65]
$[Eu(BH_4)(THF)_5]$ $[BPh_4]$	[a]	[a]	458	[23]
$Eu(BH_4)_2$	[a]	[a]	465	[24]
$Sr(BH_4)_{1.74}Cl_{0.26}$	2.96 – 3.14	3.02	457	this work
$CsEu(BH_4)_3$	[a]	[a]	485	[24]
$CsCa(BH_4)_3$	[a]	[a]	485	[24]
$CsSr(BH_4)_{2.74}Cl_{0.26}$	2.84 – 3.24	3.01	486	this work
$KSr(BH_4)_{2.80}Cl_{0.20}$	2.71 – 3.54	3.06	488	this work
$[Eu(BH_4)_2(THF)_2]$	[a]	[a]	490	[23]
$[Eu(BD_4)_2(THF)_2]$	[a]	[a]	490	[23]
Sr_2SiO_4	3.15 – 4.22	3.79	490 [c]	[66]
$RbSr(BH_4)_{2.86}Cl_{0.14}$	2.38 – 3.65	3.00	492	this work
SrSe	3.12	3.12	564	[67]
$LiSr_4[BO_3]_3$	3.26	3.26	588 [c]	[68]
SrS	3.01	3.01	620	[69]
SrO	2.61	2.61	625	[70]

[a] not reported [b] $[BO_4]_5$- units [c] second polyhedron with other CN than 6 [d] second and third polyhedron with other CN than 6

Combined with the high quantum yields and thermally stable luminescence, the Eu^{2+}-activated chloride borohydrides may be considered as potential luminescent thermometers. The vast majority among the currently still developed luminescent thermometers work with luminescence intensity ratios as those signals are stable towards absolute uncertainties of the intensity, but merely depend on relative intensity uncertainties only. In contrast, the most prominent thermal response of the presented three chloride borohydrides $ASr(BH_4)_{3-x}Cl_x:Eu^{2+}$ (*A* = K, Rb, Cs) is the emission band shift. A figure of merit for the performance of a luminescent thermometer is the relative sensitivity, which relates its thermal response to the corresponding signal at a given temperature.[71,72] Specifically, it reads for any band shift

$$S_r(T) = \left|\frac{1}{E_{em}}\frac{\partial E_{em}}{\partial T}\right| = \left|\frac{1}{\lambda_{em}}\frac{\partial \lambda_{em}}{\partial T}\right| \quad (5)$$

with E_{em} and λ_{em} as the emission energy or wavelength at temperature *T*, respectively. It should be explicitly mentioned that the relative sensitivity is invariant with respect to the chosen quantity for the emission position (E_{em} and λ_{em}). The relative sensitivity readily allows to compare different thermometers irrespective of their underlying operating principle. With eq. (5), maximum relative sensitivities of S_r = 2.85 x 10^{-2} % · K^{-1} for *A* = K (at 245 K), S_r = 2.12 x 10^{-2} % · K^{-1} for *A* = Rb (at 324 K) and S_r = 1.51 x 10^{-2} % · K^{-1} for *A* = Cs (at 178 K) were derived. Given the commonly observed blue shifts of an Eu^{2+}-related emission of around 100 cm^{-1} between 10 K and 300 K,[45,46,73,74] the relative sensitivities of the $4f^65d^1 \rightarrow 4f^7$ emission in the

chloride borohydrides are about one order of magnitude larger and thus, make these compounds unique among Eu^{2+}-activated phosphors in the context of thermal emission band position response. It is noteworthy that they are even competitive to the reported relative thermal sensitivities of CdSe quantum dots (S_r = 1.59 x 10^{-2} % · K^{-1}) using the temperature-dependent emission position shift as a response signal,[75,76] while detection of the peak shift of a Nd^{3+}-based $4f^3(^4F_{3/2}$, R2) → $4f^3(^4I_{11/2}$, Z1) emission transition in the crystal field of ALa$(PO_3)_4$ (A = Li - Rb) was shown to act an order of magnitude more sensitively (S_r = 0.48 % · K^{-1}).[77]
In contrast, however, the absolute temperature-dependent luminescence intensity or fluorescence decay time of CdSe[78-80] or, more recently, Ag_2S quantum dots[81,82] have been shown to react by orders of magnitude more sensitively (S_r > 2 % · K^{-1}) to small temperature changes. Also, the usage of a luminescence intensity ratio of two emission bands using lanthanides as emitters has already been shown to response more sensitively to small temperature changes (even S_r > 10 % · K^{-1}) in various temperature regimes.[72,83-87] The reader is referred to several excellent reviews on that topic for a broad overview of this quickly emerging field.[88-92] Thus, although the presented Eu^{2+}-activated chloride borohydrides ASr$(BH_4)_{3-x}Cl_x$ (A = K, Rb, Cs) are very sensitive in terms of their temperature-dependent emission band position, detection of the emission maximum as itself does not provide the thermal relative sensitivities already achievable in practical luminescent thermometers. This circumstance is related to the type of detected temperature response (energy or wavelength shift) itself being much lower than the reference signal (energy or wavelength). It is, however, similarly possible to quantify the blueshift by means of an analogous ratiometric area analysis. By integration of the low- and high-energy side of the temperature-dependent emission spectra (see Figs. S28 and S29 in the Supporting Information), which mimics the usage of corresponding bandpass filters, it is possible to achieve an alternative quantification for the blueshift. A similar operating principle is used by ratio pyrometers that detect the emitted black body radiation of any object at two different wavelengths. If R denotes the ratio between the integrated intensity of the high-energy portion I_2 and low-energy portion I_1, the corresponding relative sensitivity may be given by

$$S_r(T) = \left|\frac{1}{R}\frac{\partial R}{\partial T}\right| \quad (6)$$

The thus obtained relative thermal sensitivities are much higher and read S_r = 0.91 % · K^{-1} for A = K (at 211 K), S_r = 0.66 % · K^{-1} for A = Rb (at 278 K) and S_r = 0.83 % · K^{-1} for A = Cs (at 229 K). In fact, they are even competitive with convential ratiometric thermometers (S_r ≥ 1 % · K^{-1}) using two emission transitions from thermally coupled excited states.[88-93] In that sense, the presented compounds are also promising single-band luminescent thermometers.

Properties of $Sr(BH_4)_{1.74}Cl_{0.26}$:Eu^{2+}

In addition to the ternary strontium borohydride chlorides, the binary compound can be synthesized in the same manner. After ball milling of 2 equivalents $LiBH_4$ with $SrCl_2$ (2 mol% EuH_2) the blue emitting phosphor $Sr(BH_4)_{1.74}Cl_{0.26}$:Eu^{2+} is obtained and its photoluminescence emission spectrum reveals a broad emission band with a maximum at 457 nm at room temperature (see Fig. S15 in the Supporting Information). Rietveld refinement, crystallographic information, photoluminescence excitation and decay measurements can be viewed in the Supporting Information. Similar to the ternary compounds a high quantum yield of 82% is achieved.
Expectedly, the bond lengths in the binary compound $Sr(BH_4)_{1.84}Cl_{0.26}$ are more isotropic and generally shorter due to the lack of a repulsive alkali cation and thus, the coordination sphere of Eu^{2+} is closer to a perfect octahedral symmetry. Accordingly, a more blueshifted excitation band compared to the presented ternary representatives should be expected due to the

https://doi.org/10.1021/acs.chemmater.9b03048

recovery of degenerate $4f^6 5d^1(t_{2g})$ crystal field states, as is also observed (*cf*. Figure S15 in the supporting information). A similar model was already presented to explain the difference between the photoluminescence of Eu^{2+} in the iodides $CsCaI_3$ compared to $CsMgI_3$ and $CsSrI_3$, respectively.[46]

Conclusion

The mixed metal borohydride chlorides $ASr(BH_4)_{3-x}Cl_x$ (*A* = K, Rb, Cs) and $Sr(BH_4)_{1.74}Cl_{0.26}$ have been synthesized by mechanochemical reaction. These borohydride host show very efficient luminescence at room temperature upon doping with 2 mol% europium and very low thermal quenching. All mixed metal borohydride chlorides show thermally induced significant shifts of the emission energies and also a unique sensitivity towards local changes even in the second coordination sphere. In addition, the $4f^6 5d^1 \rightarrow 4f^7$ emission of the Eu^{2+}-activated ternary chloride borohydrides shows thermally induced blueshifts in the order of 1000 to 1500 cm^{-1} so far never observed for Eu^{2+} to the best of our knowledge, which makes them promising candidates for temperature sensing applications in a relevant temperature regime (200 K – 500 K), e.g. for the *in situ* studies of hydrogenation reactions. Despite the fact that the relative thermal sensitivity of this blueshift is below the much better optimized ratiometric or luminescence decay time thermometers, it is competitive to even quantum dot-based thermometers with the same operating principle of a thermally induced change in emission position.

The unusual temperature-dependent behaviour of the emission maximum is correlated to the lattice expansion of the host and especially to the temperature – dependent behaviour of the bond lengths between Eu^{2+} and the surrounding $[BH_4]^-$ units. At low temperatures, bond length anisotropy gives a deviation from perfect octahedral symmetry of the coordination sphere of the Eu^{2+} ions and redshifts the $4f^6 5d^1 \rightarrow 4f^7$ emission. Upon increasing the temperature, the collective vibrational motion of the host crystal systematically makes the Eu-B bonds more isotropic in thermal average, leading to a recovery of the octahedral symmetry. This explanation is in good agreement with the observation that the thermal expansion coefficients α_V decrease from *A* = K to *A* = Cs, consistent with the different magnitudes of blue shifts observed for these compounds. In summary, the differences of the Eu^{2+} emission for the different compounds and their thermal behaviour impressively show the potential of the optical properties of Eu^{2+} as a local structure sensor. The incorporation of these phosphors into polymer-based matrices to protect them from moisture and air should principally be feasible and will be investigated in the future with suitable polymers.

Supporting Information. Additional data on the thermal shifts, X-ray studies and lifetime measurements of the mixed metal borohydride chlorides can be viewed in the supporting information. This material is available free of charge via the Internet at http://pubs.acs.org.

Corresponding Author

* nathalie.kunkel@uni-goettingen.de

Author Contributions

The manuscript was written through contributions of all authors. All authors have given approval to the final version of the manuscript.

Funding Sources

This research was supported by a Liebig fellowship including doctoral fellowship of the Fonds der Chemischen Industrie (FCI), grant nr. 197/02, the German Research Foundation (DFG, KU 3427/4-1) and the Bavarian-French Academy Center for a Mobility aid (Az. FK03_2017). M. S., B. V. and A. M. acknowledge funding from the European Union Horizon 2020 FET-Open project NanoTBTech (grant agreement no.: 801305).

https://doi.org/10.1021/acs.chemmater.9b03048

Acknowledgement

N.K. and T. W. would like to thank Prof. Fässler for hosting our group, P. Walke for help with DSC measurements, Dr. C. Jandl for help with quantum yield measurements, Dr. W. Klein and Dr. V. Hlukhyy for help with the temperature dependent XRD measurements and C. Kriebisch as well as K. Weber for help with the syntheses.

References

(1) P. Pust, V. Weiler, C. Hecht, A. Tücks, A. S. Wochnik, A.-K. Henß, D. Wiechert, P. J. Schmidt and W. Schnick, Narrow-band red-emitting $Sr[LiAl_3N_4]:Eu^{2+}$ as a next-generation LED-phosphor material, *Nat. Mat.* **2014**, 13, 891.

(2) P. F. Smet and J. J. Joos, Stabilizing colour and intensity, *Nat. Mat.* **2017**, 16, 500.

(3) P. Strobel, C. Maak, V. Weiler, P. J. Schmidt and W. Schnick, Ultra-narrow-band blue-emitting oxoberyllates $AELi_2[Be_2O_6]:Eu^{2+}$ (AE = Sr, Ba) Paving the way to efficient RGB pc-LEDs, *Angew. Chem. Int. Ed.* **2018**, 57, 8739.

(4) G. J. Hoerder, M. Seibald, D. Baumann, T. Schröder, S. Peschke, P. C. Schmid, T. Tyborski, P. Pust, I. Stoll, M. Bergler, C. Patzig, S. Reißaus, M. Krause, L. Berthold, T. Höche, D. Johrendt and H. Huppertz, $Sr[Li_2Al_2O_2N_2]:Eu^{2+}$ - A high performance red phosphor to brighten the future, *Nat. Commun.* **2019**, 10, 1824.

(5) J. Zhou, Q. Liu and Z. Xia, Structural construction and photoluminescence tuning via energy transfer in apatite-type solid-state phosphors, *J. Mater. Chem. C* **2018**, 6, 4371.

(6) R. Kolesov, K. Xia, R. Reuter, R. Stöhr, A. Zappe, J. Meijer, P. R. Hemmer and J. Wrachtrup, Optical detection of a single rare-earth ion in a crystal, *Nat. Commun.* **2012**, 3, 1029.

(7) J. Xu, D. Murata, J. Ueda and S. Tanabe, Near-infrared long persistent luminescence of Er^{3+} in garnet for the third bio-imaging window, *J. Mater. Chem. C* **2016**, 4, 11096.

(8) J. Xu, D. Murata, Y. Katayama, J. Ueda and S. Tanabe, Cr^{3+}/Er^{3+} co-doped $LaAlO_3$ perovskite phosphor: a near-infrared persistent luminescent probe covering the first and third biological window, *J. Mater. Chem. B* **2017**, 5, 6385.

(9) R. T. Wegh, H. Donker, K. D. Oskam and A. Meijerink, Visible Quantum Cutting in $LiGdF_4:Eu^{3+}$ Through Downconversion, *Science* **1999**, 283, 663.

(10) C. D. Brites, X. Xie, M. L. Debasu, X. Qin, R. Chen, W. Huang, J. Rocha, X. Liu and L. D. Carlos, Instantaneous ballistic velocity of suspended Brownian nanocrystals measured by upconversion nanothermometry, *Nat. Nanotechnol*. **2016**, 11, 851.

(11) N. Kunkel and P. Goldner, Recent advances in rare earth doped inorganic crystalline materials for quantum information processing, *Z .Anorg. Allg. Chem.* **2018**, 644, 66.

(12) X. Qin, X. Liu, W. Huang, M. Bettinelli and X. Liu, Lanthanide-activated phosphors based on 4f-5d optical transitions: Theoretical and experimental aspects, *Chem. Rev.* **2017**, 177, 4488.

(13) G. Li, Y. Tian, Y. Zhao and J. Lin, recent progress in luminescence tuning of Ce^{3+} and Eu^{2+}-activated phosphors for pc-LEDs, *Chem. Soc. Rev.* **2015**, 44, 8688.

(14) P. Dorenbos, Energy of the first $4f^7 \rightarrow 4f^6 5d$ transition of Eu2+ in inorganic compounds, *J. Lumin.* **2003**, 104, 239.

(15) P. Dorenbos, Ce^{3+} 5d-centroid shift and vacuum referred 4f-electron binding energies of all lanthanide impurities in 150 different compounds, *J. Lumin.* **2013**, 135, 93.

(16) H. A. Höppe, H. Lutz, P. Morys, W. Schnick and A. Seilmeier, Luminescence in Eu^{2+}-doped $Ba_2Si_5N_8$: Fluorescence, thermoluminescence, and upconversion, *J. Phys. Chem. Solids* **2000**, 61, 2000.

(17) N. Kunkel and T. Wylezich, Recent advances in rare earth-doped yydrides, *Z. Anorg. Allg. Chem.* **2019**, 645, 137-145.

(18) N. Kunkel, A. Meijerink and H. Kohlmann, Bright yellow and green Eu(II) luminescence and vibronic fine structures in $LiSrH_3$, $LiBaH_3$ and their corresponding deuterides, *Phys. Chem. Chem. Phys.* **2014**, 16, 4807.

(19) N. Kunkel, R. Böttcher, T. Pilling, H. Kohlmann and A. Pöppl, Eu^{2+}-containing luminescent perovskite-type hydrides studied by electron paramagnetic resonance, *Z. Phys. Chem.* **2016**, 230, 931.

(20) N. Kunkel, A. D. Sontakke, S. Kohaut, B. Viana and P. Dorenbos, Thermally simulated luminescence and first-principle study of defect configurations in the perovskite-type hydrides $LiMH_3:Eu^{2+}$ (M = Sr, Ba) and the corresponding deuterides*, J. Phys. Chem. C*, **2016**, 120, 29141.

(21) G. Lefevre, A. Herfurth, H. Kohlmann, A. Sayede, Th. Wylezich, S. Welinski, P. Duarte Vaz, S. F. Parker, J. F. Blach, Ph. Goldner and N. Kunkel, Phonon-electron coupling in luminescent europium doped hydride perovskites studied by luminescence spectroscopy, inelastic neutron scattering, and first-principle calculations, *J. Phys. Chem. C* **2018**, 122, 10501

(22) Th. Wylezich, R. Böttcher, A. Sontakke, V. Castaing, B. Viana, A. Pöppl and N. Kunkel, Lanthanide ions as local probes in ionic hydrides: A pulsed Electron Nuclear Double Resonance and thermoluminescence study of Eu^{2+}-doped hydride perovskites, *J. Phys. Chem. C* **2019**, 123, 5031.

(23) S. Marks, J. G. Heck, M. H. Habicht, P. Oña-Burgos, C. Feldmann and P. W. Roesky, $[Ln(BH_4)_2(THF)_2]$ (Ln = Eu, Yb) - A highly luminescent material. Synthesis, properties, reactivity, and NMR studies, *J. Am. Chem. Soc.* **2012**, 134, 16983.

(24) P. Schouwink, M. B. Ley, A. Tissot, H. Hagemann, T. R. Jensen, L. Smrčok and R. Černý, Structure and properties of complex hydride perovskite materials, *Nat. Commun.* **2014**, 5, 5706.

(25) M. Paskevicius, L. H. Jepsen, P. Schouwink, R. Černý, D. B. Ravnsbæk, J. Filinchuk, M. Dornheim, F. Besenbacher and T. R. Jensen, Metal borohydrides and derivatives – synthesis, structure and properties, *Chem. Soc. Rev.* **2017**, 46, 1565.

(26) N. Kunkel and H. Kohlmann, Ionic mixed hydride fluoride compounds: Stabilities predicted by DFT, synthesis, and luminescence of divalent europium, *J. Phys. Chem. C* **2016**, 120, 10506.

(27) C. Pflug, A. Franz and H. Kohlmann, Crystal structure and europium luminescence of $NaMgH_{3-x}F_x$, *J. Solid State Chem.* **2018**, 258, 391.

(28) T. Wylezich, S. Welinski, M. Hoelzel, P. Goldner and N. Kunkel, Lanthanide luminescence as a local probe in mixed anionic hydrides – a case study on Eu^{2+}-doped $RbMgH_xF_{3-x}$ and $KMgH_xF_{3-x}$, *J. Mater. Chem. C* **2018**, 6, 13006.

(29) N. Kunkel, D. Rudolph, A. Meijerink, S. Rommel, R. Weihrich, H. Kohlmann and T. Schleid, Green luminescence of divalent europium in the hydride chloride EuHCl, *Z. Anorg. Allg. Chem.* **2015**, 641, 1220.

(30) D. Rudolph, T. Wylezich, A. D. Sontakke, A. Meijerink, P. Goldner, P. Netzsch, H. A. Höppe, N. Kunkel and T. Schleid, Synthesis and optical properties of the Eu^{2+}-doped alkaline-earth metal hydride chlorides $AE_7H_{12}Cl_2$ (AE = Ca and Sr), *J. Lumin.* **2019**, 209, 150.

(31) D. Rudolph, D. Enseling, T. Jüstel and T. Schleid, Crystal Structure and luminescence properties of the first hydride oxide chloride with divalent europium: $LiEu_2HOCl_2$ *Z. Anorg. Allg. Chem.* **2017**, 643, 1525.

(32) F. Gehlhaar, R. Finger, N. Zapp, M. Bertmer and H. Kohlmann, $LiSr_2SiO_4H$, an air-stable hydride as host for Eu(II) luminescence. *Inorg. Chem.* **2018**, 57, 11851.

(33) J. Ueda, S. Matsuishi, T. Tokunaga and S. Tanabe, Preparation, electronic structure of gadolinium oxyhydride and low-energy 5d excitation band for green luminescence of Tb^{3+} ions, *J. Mater. Chem. C* **2018**, 6, 7541.

(34) M. D. Banus, R. W. Bragdon and A. A. Hinckley, Potassium, rubidium and cesium borohydride, *J. Am. Chem. Soc.* **1954**, 76, 3848.

(35) Topas Version 5, Bruker AXS, www.bruker-axs.com, General profile and structure analysis software for powder diffraction data, Karlsruhe.

(36) A. A. Coelho, Indexing of Powder Diffraction Patterns by Iterative Use of Singular Value Decompsotion. *J. Appl. Crystallogr.* **2003**, 36, 86.

(37) D. Ravnsbæk, Y. Filinchuk, Y. Cerenius, H. J. Jakobsen, F. Besenbacher, J. Skibsted and T. R. Jensen, A series of mixed-metal borohydrides, *Angew. Chem. Int. Ed.*, **2009**, 48, 6659.

(38) E. Grube, C. H. Olesen, D. B. Ravnsbæk and T. R. Jensen, Barium borohydride chlorides: synthesis, crystal structure and thermal properties, *Dalton Trans.*, **2016**, 45, 8291.

(39) D. B. Ravnsbæk, E. A. Nickels, R. Černý, C. H. Olesen, W. I. F. David, P. P. Edwards, Y. Filinchuk and T. R. Jensen, Novel alkali earth borohydrides $Sr(BH_4)_2$ and borohydride-chloride $Sr(BH_4)Cl$, *Inorg. Chem.*, **2013**, 52, 10877.

(40) M. B. Ley, S. Boulineau, R. Janot, Y. Filinchuk and T. R. Jensen, New Li ion conductors and solid state hydrogen storage materials: $LiM(BH_4)_3Cl$, M = La, Gd, *J. Phys. Chem. C* **2012**, 116, 21267.

(41) K. T. Møller, M. B. Ley, P. Schouwink, R. Černý and T. R. Jensen, Synthesis and thermal stability of perovskite alkali metal strontium borohydrides, *Dalton Trans.*, **2016**, 45, 831.

(42) R. Shannon, Revised effective ionic radii and systematic studies of interatomic distances in halides and chalcogenides, *Acta Crystallogr., Sect. A* **1976**, 32, 751.

(43) D. H. Gahane, N. S. Kokode, B. M. Bahirwar, S. V. Moharil, Luminescence of Eu^{2+} in some chlorides, *Phys. Proc.* **2012**, 29, 42.

(44) V. L. Cherginets, N. V. Rebrova, A. Yu. Grippa, Yu. N. Datsko, T. V. Ponomarenko, V. Yu. Pedash, N. N. Kosinov, V. A. Tarasov, O. V. Zelenskaya, I. M. Zenya, A. V. Lopin, Scintillation properties of $CsSrX_3:Eu^{2+}$ ($CsSr_{1-y}Eu_yX_3$, X = Cl, Br; $0 \le y \le 0.05$) single crystals grown by the Bridgman method, *Mater. Chem. Phys.* **2014**, 143, 1296.

(45) M. Suta, P. Larsen, F. Lavoie-Cardinal and C. Wickleder, Photoluminescence of $CsMBr_3:Eu^{2+}$ (M=Mg, Ca, Sr)-A novel strategy for the development of low-energy emitting phosphors, *J. Lumin.*, **2014**, 149, 35.

(46) M. Suta and C. Wickleder, Photoluminescence of $CsMI_3:Eu^{2+}$ (M = Mg, Ca, and Sr) – a spectroscopic probe on structural distortions, *J. Mater. Chem. C*, **2015**, 3, 5233.

(47) K. Huang and A. Rhys, Theory of light absorption and non-radiative transitions in *F*-centres, *Proc. R. Soc. Lond. A*, **1950**, 204, 406.

(48) M. de Jong, L. Seijo, A. Meijerink and F. T. Rabouw, Resolving the ambiguity in the relation between Stokes shift and Huang-Rhys parameter, *Phys. Chem. Chem. Phys.*, **2015**, 17, 16959.

(49) P. Schouwink, H. Hagemann, J. P. Embs, V. D'Anna and R. Černý, Di-hydrogen contact induced lattice instabilities and structural dynamics in complex hydride perovskites, *J. Phys.: Condens. Matter* **2015**, 27, 265403.

(50) T. Kobayashi, S. Mroczkowski, J. F. Owen and L. H. Brixner, Fluorescence lifetime and quantum efficiency for 5d → 4f transitions in Eu^{2+} doped chloride and fluoride crystals, *J. Lumin.* **1980**, *21*, 247.

(51) S. H. M. Poort, A. Meijerink and G. Blasse, Lifetime measurements in Eu^{2+}-doped host lattices, *J. Phys. Chem. Solids* **1997**, 58, 1451.

(52) J. M. F. van Dijk and M. F. H. Schuurmans, On the nonradiative and radiative decay rates and a modified exponential energy gap law for 4*f*-4*f* transitions in rare earths, *J. Chem. Phys.* **1983**, 78, 5317.

(53) M. Suta and C. Wickleder, Spin crossover of Yb^{2+} in $CsCaX_3$ and $CsSrX_3$ – A guideline to novel halide-based scintillators, *Adv. Funct. Mater.* **2016**, 27, 1602783.

(54) T. Senden, F. T. Rabouw and A. Meijerink, Photonic effects on the radiative decay rate and luminescence quantum yield of doped nanocrystals, *ACS Nano* **2015**, 9, 1801.

https://doi.org/10.1021/acs.chemmater.9b03048

(55) S. Yan, On the origin of temperature dependence of the emission maxima of Eu^{2+} and Ce^{3+} -activated phosphors, *Opt. Mater.* **2018**, 79, 172.

(56) W. T. Carnall, G. L. Goodman, K. Rajnak and R. S. Rana, A systematic analysis of the spectra of the lanthanides doped into single crystal LaF_3, *J. Chem. Phys.*, **1989**, 90, 3443.

(57) M. Widenmeyer, R. Niewa, T. C. Hansen and H. Kohlmann, In situ neutron diffraction as a probe for formation and decompositions of nitrides and hydrides: A case study, *Z. Anorg. Allg. Chem.* **2013**, 639, 285.

(58) C. Abraham, B. Fond, A. L. Heyes and F. Beyrau, High-speed planar thermometry and velocimetry using thermographic phosphor particles*, Appl. Phys. B* **2013**, 111, 155.

(59) J. Y. Sun, Q. M. Di, L. Han, Q. G. Xu and C. L. Ma, Hydrothermal synthesis of $SrSO_4:Eu^{2+}$ microcrystals with different morphologies and its luminescence properties, *Appl. Mech. Mater.*, **2014**, 633-634, 341.

(60) A. Diaz and D. A. Keszler, Red, green, and blue Eu^{2+} luminescence in solid-state borates: A structure-property relationship, *Mater. Res. Bull.*, **1996**, 31, 147.

(61) H. Ji, Z. Huang, Z. Xia, M. S. Molokeev, V. V. Atuchin, M. Fang and Y. Liu, Discovery of new solid solution phosphors via cation substitution-dependent phase transition in $M_3(PO_4)_2:Eu^{2+}$ (M = Ca/Sr/Ba) quasi-binary Sets, *J. Phys. Chem. C*, **2015**, 119, 2038.

(62) M. Hoffman, Eu activation in some alkaline earth strontium phosphate compounds, *J. Appl. Phys*., **1962**, 33, 2186.

(63) S. S. Gokhale, L. Stand, A. Lindsey, M. Koschan, M. Zhuravleva and C. L. Melcher, Improvement in the optical quality and energy resolution of $CsSrBr_3$:Eu scintillator crystals, *J. Cryst. Growth*, **2016**, 445, 1.

(64) K. Yang, M. Zhuravleva and C. L. Melcher, Crystal growth and characterization of $CsSr_{1-x}Eu_xI_3$ high light yield scintillators, *Phys. Status Solidi RRL*, **2011**, 5, 43.

(65) D. K. Yim, H. J. Song, I.-S. Cho, J. S. Kim and K. S. Hong, A novel blue-emitting $NaSrPO_4:Eu^{2+}$ phosphor for near UV based white light-emitting-diodes, *Mater. Lett.*, **2011**, 65, 1666.

(66) J. S. Kim, Y. H. Park, S. M. Kim, J. C. Choi and H. L. Park, Temperature-dependent emission spectra of $M_2SiO_4:Eu^{2+}$ (M=Ca, Sr, Ba) phosphors for green and greenish white LEDs, *Solid State Commun.*, **2005**, 133, 445.

(67) X. Zhang, L. Liang, J. Zhang and Q. Su, Luminescence properties of $(Ca_{1-x}Sr_x)Se:Eu^{2+}$ phosphors for white LEDs application, *Mater. Lett.*, **2005**, 59, 749.

(68) H. Yu, D. Deng, Y. Hua, C. Li and S. Xu, Orange- to green-emitting $Li(Sr,Ca)_4(BO_3)_3:Eu^{2+}$ phosphor: emission-tunable properties and white light emitting diode application, *RSC Advances*, **2016**, 6, 82824.

(69) Q. Xia, M. Batentschuk, A. Osvet, P. Richter, D. P. Häder, J. Schneider, L. Wondraczek, A. Winnacker and C. J. Brabec, Red-emitting $Ca_{1-x}Sr_xS:Eu^{2+}$ phosphors as light converters for plant-growth applications, *Mater. Res. Soc. Symp. Proc.*, **2011**, 1342, mrss11-1342-v1304-1304.

(70) N. Yamashita, Photoluminescence spectra of the Eu^{2+} center in SrO:Eu, *J. Lumin.*, **1994**, 59, 195.

(71) S. F. Collins, G. W. Baxter, S. A. Wade, T. Sun, K. T. V. Grattan, Z. Y. Zhang, A. W. Palmer, Comparison of fluorescence-based temperature sensor schemes: Theoretical analysis and experimental validation, *J. Appl. Phys.* **1998**, 84, 4649.

(72) S. A. Wade, S. F. Collins, G. W. Baxter, Fluorescence intensity ratio technique for optical fiber point temperature sensing, *J. Appl. Phys.* **2003**, 94, 4743.

(73) O. M. Kate, R. Xie, C. Wang, S. Funahashi and N. Hirosaki, Eu^{2+}-Doped $Sr_2B_{2-2x}Si_{2+3x}Al_{2-x}N_{8+x}$: A boron-containing orange-emitting nitridosilicate with interesting composition-dependent photoluminescence properties, *Inorg. Chem*. **2016** 55, 11331.

(74) C. Liu, Z. Qi, C. Ma, P. Dorenbos, D. Hou, S. Zhang, X. Kuang, J. Zhang and H. Liang, High light yield of $Sr_8(Si_4O_{12})Cl_8:Eu^{2+}$ under X-ray excitation and its temperature-dependent luminescence characteristics, *Chem. Mater.* **2014** 26 (12), 3709.

(75) S. Li, K. Zhang, J.-M. Yang, L. Lin and H. Yang, Single quantum dots as local temperature markers, *Nano Lett.* **2007**, 7, 3102.

(76) L. M. Maestro, E. M. Rodríguez, F. S. Rodríguez, M. C. Iglesiaz-de la Cruz, A. Juarranz, R. Naccache, F. Vetrone, D. Jaque, J. A. Capobianco and J. G. Solé, CdSe quantum dots for two-photon fluorescence thermal imaging, *Nano Lett.* **2010**, 10, 5109.

(77) Ł. Marciniak, A. Bednarkiewicz, D. Hreniak and W. Strek, The influence of the Nd^{3+} concentration and alkali ions on the sensitivity of non-contact temperature measurements in $ALaP_4O_{12}:Nd^{3+}$ (A = Li, Na, K, Rb) nanocrystalline luminescent thermometers, *J. Mater. Chem. C* **2016**, 4, 11284.

(78) G. W. Walker, V. C. Sundar, C. M. Rudzinski, A. W. Wun, M. G. Bawendi and D. G. Nocera, Quantum-dot optical temperature probes, *Appl. Phys. Lett.* **2003**, 83, 3555.

(79) P. A. S. Jorge, M. Mayeh, R. Benrashid, P. Caldas, J. L. Santos and F. Farahi, Quantum dots as self-referenced optical fibre temperature probes for luminescent chemical sensors, *Meas. Sci. Technol.* **2006**, 17, 1032-1038.

(80) E. N. Cerón, D. H. Ortgies, B. del Rosal, F. Ren, A. Benayas, F. Vetrone, D. Ma, F. Sanz-Rodríguez, J. G. Solé, D. Jaque and E. M. Rodríguez, Hybrid Nanostructures for High-Sensitivity Luminescence Nanothermometry in the Second Biological Window, *Adv. Mater.* **2015**, 27, 4781-4787.

(81) H. D. A. Santos, D. Ruiz, G. Lifante, C. Jacinto, B. H. Juarez and D. Jaque, Time resolved spectroscopy of infrared emitting Ag_2S nanocrystals for subcutaneous thermometry, *Nanoscale* **2017**, 9, 2505-2513.

(82) B. del Rosal, D. Ruiz, I. Chaves-Coira, B. H. Juárez, L. Monge, G. Hong, N. Fernandez and D. Jaque, In Vivo Contactless Brain Nanothermometry, *Adv. Funct. Mater.* **2018**, 28, 1806088.

https://doi.org/10.1021/acs.chemmater.9b03048

(83) X. Liu, S. Akerboom, M. de Jong, I. Mutikainen, S. Tanase, A. Meijerink and E. Bouwman, Mixed-Lanthanoid Metal-Organic Framework for Ratiometric Cryogenic Temperature Sensing, *Inorg. Chem.* **2015**, 54, 11323.

(84) D. Ananias, F. A. A. Paz, L. D. Carlos and J. Rocha, Near-Infrared Ratiometric Luminescent Ratiometric Thermometer Based on a New Lanthanide Silicate, *Chem. Eur. J.* **2018**, 24, 11926.

(85) E. C. Ximendes, U. Rocha, T. O. Sales, N. Fernández, F. Sanz-Rodríguez, I. R. Martín, C. Jacinto and D. Jaque, In vivo subcutaneous thermal video recording by supersensitive infrared nanothermometers, *Adv. Funct. Mater.* **2017**, 27, 1702249.

(86) Ł. Marciniak, A. Bednarkiewicz and K. Elzbieciak, NIR-NIR photon avalanche based luminescent thermometry with Nd^{3+} doped nanoparticles, *J. Mater. Chem. C* **2018**, 6, 7568.

(87) E. C. Ximendes, A. F. Pereira, U. Rocha, W. F. Silva, D. Jaque and C. Jacinto, Thulium doped LaF_3 for nanothermometry operating over 1000 nm, *Nanoscale* **2019**, 11, 8864.

(88) D. Jaque and F. Vetrone, Luminescence Nanothermometry, *Nanoscale* **2012**, 4, 4301.

(89) C. D. S. Brites, P. P. Lima, N. J. O. Silva, A. Millán, V. S. Amaral, F. Palacio and L. D. Carlos, Thermometry at the nanoscale **2012**, **4**, 4799.

(90) C. D. S. Brites, A. Millán and L. D. Carlos, *Lanthanides in Luminescence Thermometry* (Ch. 281), in : Handbook on the Physics and Chemistry of Rare Earths (eds.: J.-C. Bünzli, V. Pecharsky) **2016**, Vol. 49, pp. 339-427, Elsevier, Amsterdam.

(91) M. D. Dramićanin, Sensing temperature via downshifting emissions of lanthanide-doped metal oxides and salts. A review, *Meth. Appl. Fluoresc.* **2016**, 4, 042001.

(92) C. D. S. Brites, S. Balabhadra and L. D. Carlos, Lanthanide-based thermometers: At the cutting-edge of luminescence thermometry, *Adv. Opt. Mater.* **2019**, 7, 1801239.

(93) D. Errulat, R. Marrin, D. A. Gálico, K. L. M. Harriman, A. Pialat, B. Gabidullin, F. Iikawa, O. D. D. Couto, Jr., J. O. Moilanen, E. Hemmer, F. A. Sigoli, M. Murugesu, A luminescent thermometer exhibiting slow relaxation of the magnetization: Toward self-monitored building blocks for the next-generation optomagnetic devices, *ACS Centr. Sci.* **2019**, 5, 1187.

https://doi.org/10.1021/acs.chemmater.9b03048